Solid State Ionics 286 (2016) 72–82

Contents lists available at ScienceDirect

Solid State Ionics

journal homepage: www.elsevier.com/locate/ssi

Forcespinning: A new method for the mass production of Sn/C composite nanofiber anodes for lithium ion batteries

Victor A. Agubra, Luis Zuniga, David De la Garza, Luis Gallegos, Madhab Pokhrel, Mataz Alcoutlabi *

Department of Mechanical Engineering, University of Texas, Rio Grande Valley, Edinburg, TX 78539, United States

ARTICLE INFO

Article history:
Received 10 September 2015
Received in revised form 5 November 2015
Accepted 2 December 2015
Available online xxxx

Keywords:
Lithium ion battery
Anodes
Carbon nanofibers
Forcespinning
Composite electrode
Tin

ABSTRACT

The development of nanostructured anode materials for rechargeable Lithium-ion Batteries has seen a growing interest. We herein report the use of a new scalable technique, Forcespinning (FS) to produce binder-free porous Sn/C composite nanofibers with different Sn particle size loading. The preparation process involves the FS of Sn/PAN precursor nanofibers and subsequently stabilizing in air at 280 °C followed by carbonization at 800 °C under an inert atmosphere. The Sn/C composite nanofibers are highly flexible and were directly used as binder-free anodes for lithium-ion batteries. The produced Sn/C composite nanofibers showed an improved discharge capacity of about 724 mA h g^{-1} at a current density of 100 mA g^{-1} for over 50 cycles compared to most nanofiber electrodes prepared by electrospinning and centrifugal spinning. The FS method clearly produces Sn/C nanofiber composite electrodes that have a high specific capacity and excellent cyclic performance, owing to the unique structure and properties of the nanofibers. The FS technology is thus a viable method for the large scale production of nano/micro fibers for battery electrodes, separators, and other applications. To the best of our knowledge, this is the first time to report results on the use of Forcespinning technology to produce composite nanofiber anodes for lithium-ion batteries.

1. Introduction

Recently there has been an increase in research activities focusing on the development of nanostructured materials [1] as anodes to enhance the capacity, energy density and specific power of rechargeable Lithium-ion Batteries (LIBs) [2–7]. In the early development of the lithium battery chemistry, lithium metal foil was widely used as the anode material because of several electrochemical attributes; light weight, high voltage, and high energy density. However, its propensity to form lithium dendrites and moss that can negatively impact the battery capacity retention has led to its limited use in commercial lithium ion batteries. Because of these limitation and safety issues of lithium metal as anode material, it has been replaced by several anode materials such as; graphite, coke, hard carbon, highly ordered pyrolytic graphite and lithium titanate which are less susceptible to dendrite and moss formation [8,9].

The cathode material generally has a capacity about half of the widely used carbonaceous anode material. Although the rate at which the increase in total battery capacity depends on the cathode capacity, a noticeable improvement in the overall battery capacity is often observed when an alternate anode material having a capacity of the order of 1000 mA g^{-1} is employed. There exist several viable alternative materials with much higher theoretical capacities than that of carbonaceous material [10–13]. Therefore, LIBs can be designed using high capacity alternative materials to compensate for the low capacity of cathode materials. The driving force for such a replacement of the carbonaceous material lie in the fact that the potential of the anode vs Li/Li^+ should be close to 0 V and not necessarily based on the type of electrochemical intercalation reaction at the anode. Alloying the Li^+ with several viable metals that alloy electrochemically well with lithium namely; Si, S, Ge, Al, Ag, Pb, and Sn, are all potential candidates that have received a lot of attention [4,14–16]. These Li_xM alloys show a much higher Li:M ratio at the end of the charge cycle therefore allowing a greater Li^+ accommodation whilst maintaining some relative crystal structure stability over several electrochemical cycles. These Li–Si or Li–Sn alloys-based ion batteries not only have a higher energy density of about 370 Wh/kg [10,13,17] compared to graphite-based Li-ion batteries (160 Wh/kg), but their structural stability and the ability to host a large amount of Li^+ are ideal for fast charging. However, these lithium alloy anodes are known to degrade rapidly from their high theoretical specific capacity of about 998–3600 mA h g^{-1} due to several factors including; a high volume change during the alloying/de-alloying process that leads to pulverization of the electrode [18–20].

Tin-based derivatives such as tin oxides, tin sulfides, and stannates have become attractive anode materials for LIBs. One such property of Sn-based anodes is their avoidance of solvent co-intercalation, and a significant improvement in safety performance over the commercial graphite anode in LIBs [12,17,21–23]. In addition, Sn-based anodes are easy to process and exhibit lower potential hysteresis compared to

* Corresponding author. Tel.: +1 956 665 8945.
E-mail address: mataz.alcoutlabi@utrgv.edu (M. Alcoutlabi).

http://dx.doi.org/10.1016/j.ssi.2015.12.020
0167-2738/

transition metal oxides [10]. Sn-based anodes can host a higher amount of lithium ions in the tin crystal structure, i.e. about four (4) atoms (i.e. Li_xSn, $0 < X \leq 4.4$) thereby giving Sn composite electrode a higher lithium storage capacity compared to graphite anode (i.e. Li_xC_6, $0 < X \leq 1$). However, the practical application of Sn-based anodes is usually hampered by its poor cyclability, due to the large volume changes of (i.e. >260%), resulting in particle isolation that can cause disconnectivity between the electrical conductive particles during the charge/discharge process.

Several efforts have been geared towards mitigating the huge initial capacity loss of Sn-based anodes [6,24–26]. One of such methods is coating the Sn composite anode with carbon. Carbon has been extensively used as a coating material for Sn composite electrodes mainly due to its high conductivity and considerable flexibility that improves the electrochemical performance of Sn/C composite [2,25,27–29]. The control of the morphology of a composite electrode is another key strategy; one of such morphological manipulation is the core/shell structure formation [30–33]. In this method, the core is typically the main active component, tin or tin-based materials, while the shell comprises of a protective layer surrounding the core material. In most cases, carbon is considered an ideal candidate for the shell coating material. The core/shell composite electrode architecture is one promising method to overcome the unstable cycling problem of the Sn-based anode electrode. The design of a novel two-dimensional carbon sheet with one atom thickness is another method to control the rapid degradation of the Sn-based composite electrode. In this technique, graphene nanosheets are extensively used since graphene is considered as an excellent buffering material to counter the volumetric changes in composite electrodes [5]. The use of Sn/C composite nanofibers as anode for LIBs to reduce the high volumetric changes in the anode is another method that has recently taken center stage [24,34,35]. The fibrous structure of Sn/C composite nanofibers provides ample room to accommodate the volume changes during the intercalation/de-intercalation process. Electrospinning is the common method that most often used to produce these nanofibers. The reported electrochemical performance of Sn/C composite anodes produced through electrospinning typically has initial capacities ranging between 700-1000 mA h g^{-1} and gradually degrading to about 400–600 mA h g^{-1} after 50 cycles [24,34–36]. In nanofiber processing such as electrospinning and Forcespinning, a polymer precursor is usually used to produce nanofibers that will be transformed into carbon nanofibers after different thermal treatments (carbonization). The resulting carbon nanofiber mats can be very often brittle. This can be avoided by carrying out a stabilization process in air (i.e. oxidative stabilization) on the polymer nanofiber precursor prior to carbonization. The yield of carbon nanofibers depends on several factors including the polymer-type used during nanofiber spinning. In general, the behavior of polymeric materials is time, temperature and pressure dependent [37,38], therefore, the nanofiber morphology and structure are significantly dependent on the polymer concentration and the chemical structure of the polymer used to prepare the nanofiber precursor. For brittle carbon nanofiber mats, the conductivity of the composite CNF electrode can be increased by grinding and mixing the carbon nanofibers with conductive carbon black and binding agent to produce a slurry for the electrode fabrication process [35,39–41]. The grinding of the uniform nanofibers rather compromises the fibrous nature of the nanofibers and its intended purpose. On the other hand, the electrospinning process has a low fiber yield of about 0.1 g/h, thus limiting the scaling up and productivity of the electrospinning process for commercial electrode applications. Centrifugal spinning is another method that has been recently employed to produce nanofibers as electrode for LIBs [42,43]. However, the in-house built centrifugal spinning system cannot be used to produce fibers at high rotational speeds and presently it has no capacity of melt spinning [24,44–49]. The Forcespinning method on the other hand can produce fibers from solution precursors at a high speed up to 12,000 r.p.m. with the capability of melt spinning at up to 25,000 r.p.m. [50].

We herein present a novel method of producing uniform and flexible nanofiber mats after carbonization (Fig. 1), known as Forcespinning developed by Sarkar, Lozano and coworkers at UTPA [51–54]. The FS technique has several features such as a fiber management system that allow tunable fiber deposition to ensure accurate cross directional coating uniformity, and also adaptable to substrate web widths. The FS system has the capability for dual materials feed thus allowing the continuous materials feed system especially for melt and solution spinning with no material dielectric requirements. Additionally, the FS system has an almost 100% yield and solvent-free processing for melt spinning with melt temperatures up to 350 °C. This thus eliminates the direct operating expense and environmental burdens. The method is capable of producing nanofiber from either solutions or pure molten materials. This FS technology requires less solvent or no solvent at all (i.e. melt Forcespinning), thereby making it a more cost effective method with better safety of operation compared to electrospinning [39,55]. Electrospinning can produce nanofibers with a low production rate and with safety concerns particularly at high current and voltage, which prevents the use of this method to mass produce nanofibers. Alcoutlabi and coworkers used previously electrospinning to fabricate nanofibers and carbon composite nanofibers for use as separators [56–60] and electrodes for LIBs [6,7,61]. The centrifugal spinning method, has been recently used to produce doughnut-form fibers for use in energy storage devices and biomedical applications [62,63]. The nanofibers produced using the FS method are collected on a fan box covered with a PP spun- bond fibers as the substrate where the fibers are deposited as nonwoven mats [64]. The collected fibrous mats were subjected to different thermal treatment with aim to produce uniform and flexible Sn/C fibers with good morphology and dispersion of Sn particles into the nanocomposite matrix. The mass production capability of the FS process makes it a suitable technique to produce, binder–free electrodes for commercial lithium alloys or second-generation anode electrodes for lithium ion batteries application.

2. Experimental

2.1. Materials

Poly(acrylonitrile) with average Mw 150,000 was purchased from Sigma Aldrich USA, while solvent N,N-dimethyl Formamide (DMF) was obtained from Fisher Scientific USA. The PAN/DMF solution was used as the precursor of carbon nanofibers. The commercial lithium foil, and the lithium hexafluorophosphate ($LiPF_6$), ethylene carbonate (EC), dimethyl carbonate (DMC), and the tri-layer layer PP/PE/PP separator were purchased from MTI corp. USA, The nano powder (Sn, 99.9%, 60–80 nm) was purchased from US research Nanomaterials while that of the Tin submicron particles (Sn 99.9%, 150 nm) was purchased from Sigma Aldrich USA and used as received.

2.1.1. Producing PAN/Sn fibrous mats

A specified amount (15 wt.%) of Tin (Sn) particles of base polymer polyacrylonitrile (PAN) was dissolved in DMF and sonicated for 30 min to obtain a homogenous dispersion of Sn particles. The base polymer, PAN (12 wt.%) was then added to the DMF/Sn solution and mechanically mixed using magnetic stirring for 24 h at room temperature. The nano-fibrous mat of PAN/Sn precursor was then prepared by FS. A thin fiber spun-bond was used on a fan box as the substrate for the deposition of fibers. In the FS technique, centrifugal force is used to extrude polymer solutions or melts through the spinneret. Fiber jets are formed at high spinneret rotational speeds up to 20,000 rpm. An amount of 2 mL of the PAN/Sn solution was injected into the needle-based spinneret equipped with 30 gauge half-inch regular bevel needles. The rotational speed of the spinneret was kept at 8000 rpm. The 2 mL PAN/Sn solution produced 0.32 g of fibers in 2 min, compared to less than 0.1 g/h produced using a typical lab scale electrospinning system. The substrate was rotated 90° after each run and the needles

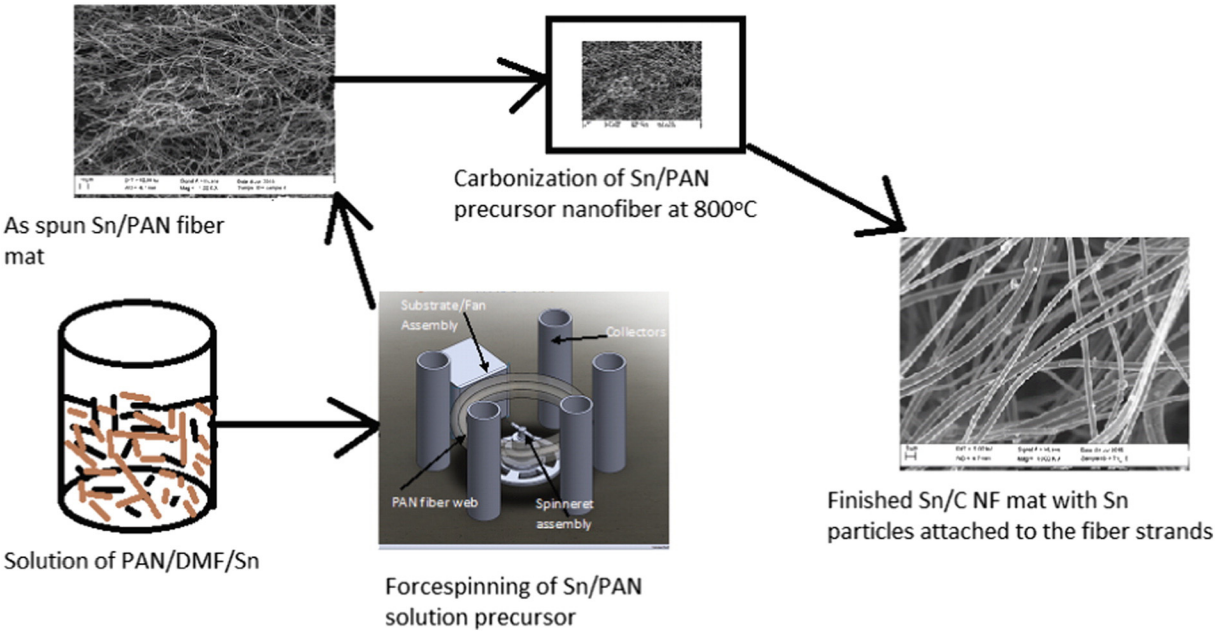

Fig. 1. A schematic diagram showing the process flow for making Sn/C nanofiber mats anodes for lithium ion batteries using Forcespinning.

were changed after each run. The PAN/Sn fibrous mats were removed from the substrate drum and dried at 120 °C under vacuum for 24 h prior to carbonization. The forcespun Sn/PAN precursor nanofibers were then stabilized in an air environment at 280 °C for 5 h (the heating rate was 3 °C min^{-1}), followed by carbonization at 800 °C for 2 h in an inert environment (i.e. argon atmosphere) to obtain a Sn/Carbon composite nanofiber mat. The Sn/PAN precursor nanofibers and Sn/carbon composite nanofibers are shown in Fig. 2. For comparison, carbon nanofibers (CNFs) made from PAN (12 wt.%) in DMF solution was also prepared.

The structure, morphology, and elemental composition of the Sn/C nanofiber mats were analyzed using scanning electron microscope (SEM) and (STEM/EDAX) from Sigma VP Carl Zeiss. While the crystal structure and the surface analysis were evaluated using X-rays powder diffraction and XPS from Bruker and Thermo Scientific respectively. The thermal and residual weight of the carbon in the Sn/PAN matrix was carried out using Thermo-Gravimetric analyzer (TGA) from TA Instruments (QA 600). The temperature was increased from 24 °C to 700 °C using a heating rat of 10 °C/min in air environment.

2.1.2. Sn/C cell assembly

Electrochemical performance evaluations were performed using 2032 coin-type cells containing Sn/C composite nanofibers with various Sn particle size and carbon nanofibers (CNFs). The cells were assembled in a high-purity argon-filled glove box (Mbraun, USA) using a pressure crimper. These CNFs and Sn/C nanofibers formed a flexible free-standing nonwoven mats, which were punched directly to be used as binder-free anodes. The anode thickness was approximately 40–60 μm with a weight average in the range of 3–5 mg. Lithium metal was used as the counter electrode and Celgard tri-layer (PP/PE/PP) membrane as the separator. The electrolyte used was a 1 M $LiPF_6$ solution in ethylene carbonate (EC)/dimethyl carbonate (DMC) (1:1 *v*/*v*). The electrochemical performance was evaluated by carrying out galvanostatic charge–discharge experiments at a current density of 100 mA/g and between 0.05 and 3.0 V. The specific charge/discharge capacities were calculated based on the mass of the of the flexible nanofiber anodes (active material). The cyclic voltammetry and electrochemical impedance experiments were evaluated using electrochemical impedance spectroscopy (Autolab 128 N) with a scan rate of 0.2 mV/s (between 0 and 3 V) and at a frequency of 0.1 Hz and 1 kHz, respectively.

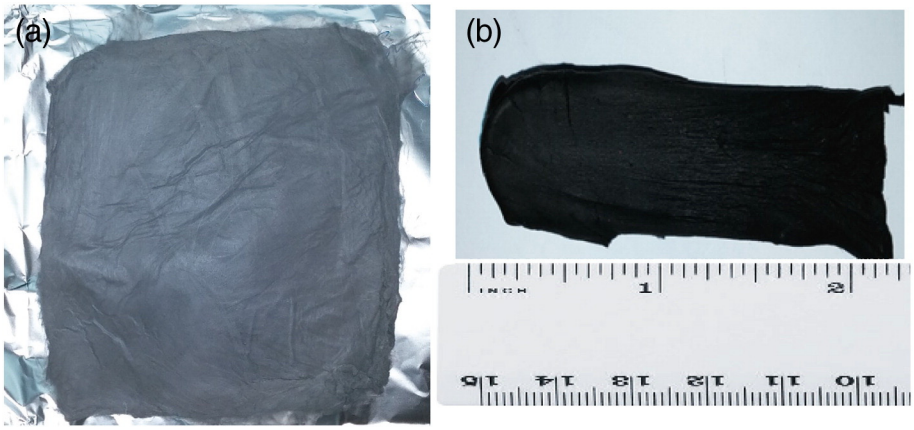

Fig. 2. Pictorial view of the Sn/PAN precursor nanofibers (a) and the Sn/C composite nanofibers prepared after carbonization at 800 °C for 3 h (b).

3. Results and discussion

3.1. Surface morphology and elemental analysis

The fibrous structure of the Sn/C composite nanofibers for both the Sn nanoparticles and the submicron particles are shown in Fig. 3 (d) and (f) respectively. SEM images of PAN precursor nanofibers (i.e. the As-Forcespun PAN fibers) and carbon nanofibers CNFs are shown in Fig. 3 (a) and (b) respectively. After carbonization at 800 °C in argon atmosphere for 2 h, the PAN fibers were transformed into carbon nanofibers (CNFs) while those of the Sn/PAN fibers transformed to Sn/C composite nanofibers. Generally, there was no variation in the fiber diameters between the baseline (PAN fibers) and the carbonized nanofibers, with the fibers diameters ranging between 200 and 600 nm. Sn particles are distributed along the Sn/C composite nanofibers and some of the particles form clusters on the fiber surface (Fig. 3(e)) with pores that are evenly distributed on the fibers as shown in Fig. 3d, and f. The pore formation was more pronounced on the mirco-particle Sn/

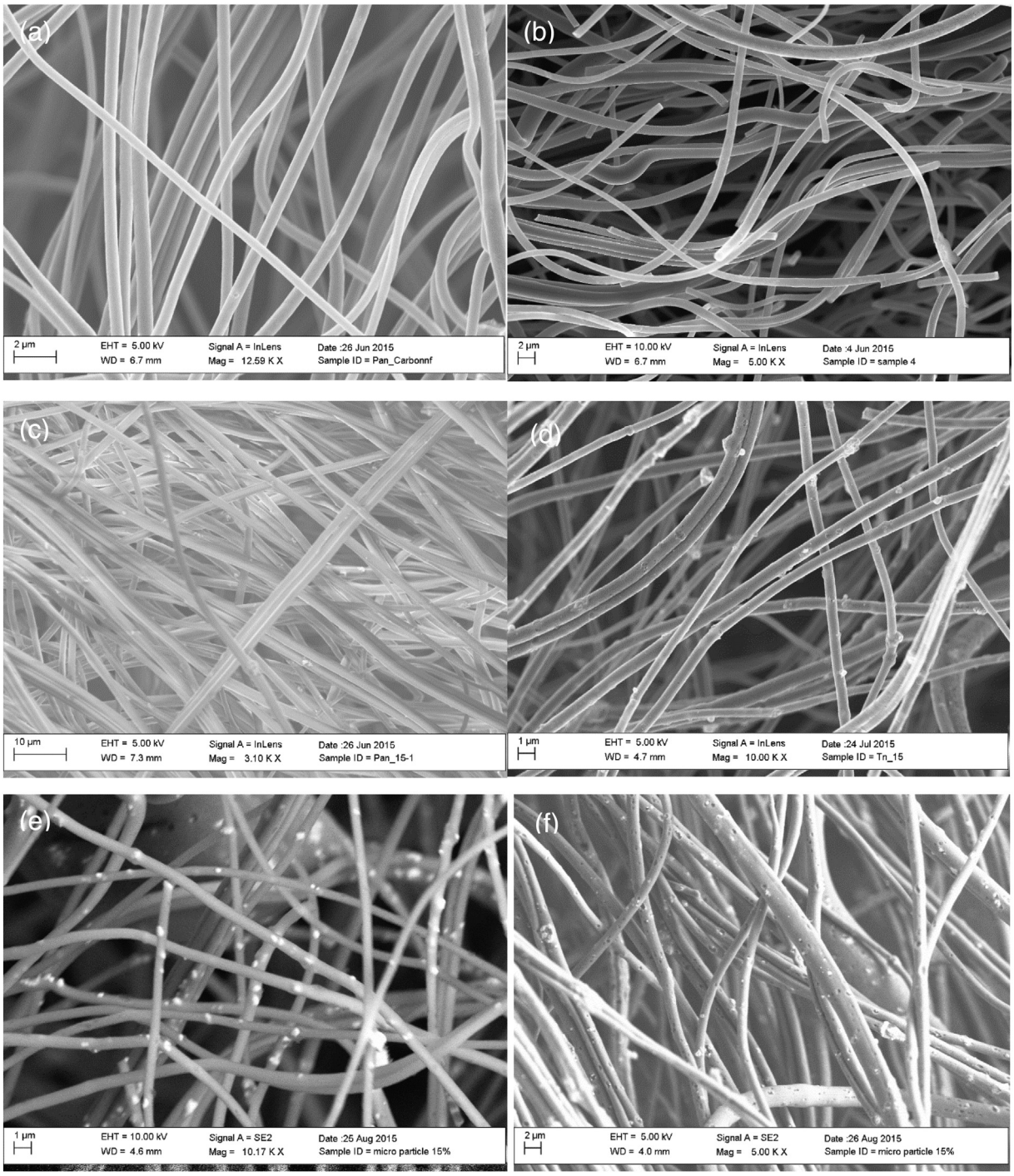

Fig. 3. SEM micrographs showing the morphology of the PAN precursor nanofibers (a) and the CNFs prepared from PAN precursor nanofibers (b), the Sn (nanoparticles)/PAN precursor nanofibers (c) and the Sn (nanoparticles)/C composite nanofibers (d), the Sn (microparticles)//PAN precursor nanofibers (e) and Sn (microparticles)//C composite nanofibers with porous structure (f).

C composite fibers compared to those on the Sn nanoparticles Sn/C composite fibers. These pores played a key role in buffering/accommodating the volume changes that accompanied the alloying and de-alloying process of Sn with lithium while small pores in porous CNFs provide additional room for Li insertion during charge. These pores on the Sn/C composite electrode do not exist on the as-forcespun fibers (Fig. 3(c) and (e)), meaning that the pores on the fibers were formed after the carbonization process. EDAX elemental analysis of the composite Sn/C nanofibers (Fig. 4a) clearly shows that the fibers predominantly consisted of Sn and carbon. The areal mapping of the Sn/C composite nanofibers (Fig. 4a) shows the distribution of the Sn nanoparticles in the carbon matrix. The area mapping clearly shows that composite the electrode predominantly consists of carbon (86% atomic weight) with Sn (14% atomic weight) where the Sn particles are heterogeneously distributed.

The actual weight of carbon in the Sn/C composite fibers was evaluated using TGA measurement. As shown in Fig. 4b, up to 92 °C, a minor weight reduction of ~3% was observed which corresponds to the removal of physically absorbed water from the fibers. At temperature between 290 °C and 410 °C, there is a multistage decomposition that could be attributed to the polymer (Polyacrylonitrile) which recorded a weight loss of ~38%. The oxidation of carbon was observed above 450 °C, and beyond 530 °C, the weight loss remains steady. The TGA results indicate that the Sn/C fibers contain ~48 wt.% carbon.

3.2. Crystal structure analysis of the Sn/C composite anode

X-ray diffraction (XRD) analysis (Fig. 5) of the as-synthesized Sn/C nanofibers clearly revealing the diffraction pattern of a tetragonal rutile structure (JCPDS 41-1445) which belongs to the space group $P4_2/mnm$ (136). In addition, a peak at 18° followed by a broad peak belongs to the un-stabilized PAN polymer.

The small peak at 18° disappears after carbonization, while the broad amorphous peak still exists after the carbonization process. This phenomenon could be attributed to the presence of hard carbon or non-graphitized carbon in the carbon fiber. During the carbonization process of Sn/PAN precursor nanofibers at 800 °C in inert atmosphere, the PAN polymer was converted into carbon fiber, while the Sn could have been oxidized to SnO_2 during the stabilization process at 250 °C and back to the metallic phase at 800 °C during the carbonization process in the inert environment. However, it is expected that a few amount of the oxide will still exist in the final product of Sn/C composite electrode. The peak pattern obtained in the X-ray shows a small amount of SnO_2 and metallic Sn. The peaks of the metallic Sn were observed as doublet at 43° in the as-forcespun Sn/PAN. The carbonization process completely separates the shoulder of the peak of the metallic Sn in the As-spun Sn/PAN nanofiber into two distinct peaks indexed as (220) and (211). Additionally, there was a slight shift of the (200) and the (101) peaks to lower 2θ relative to the baseline, that could be an

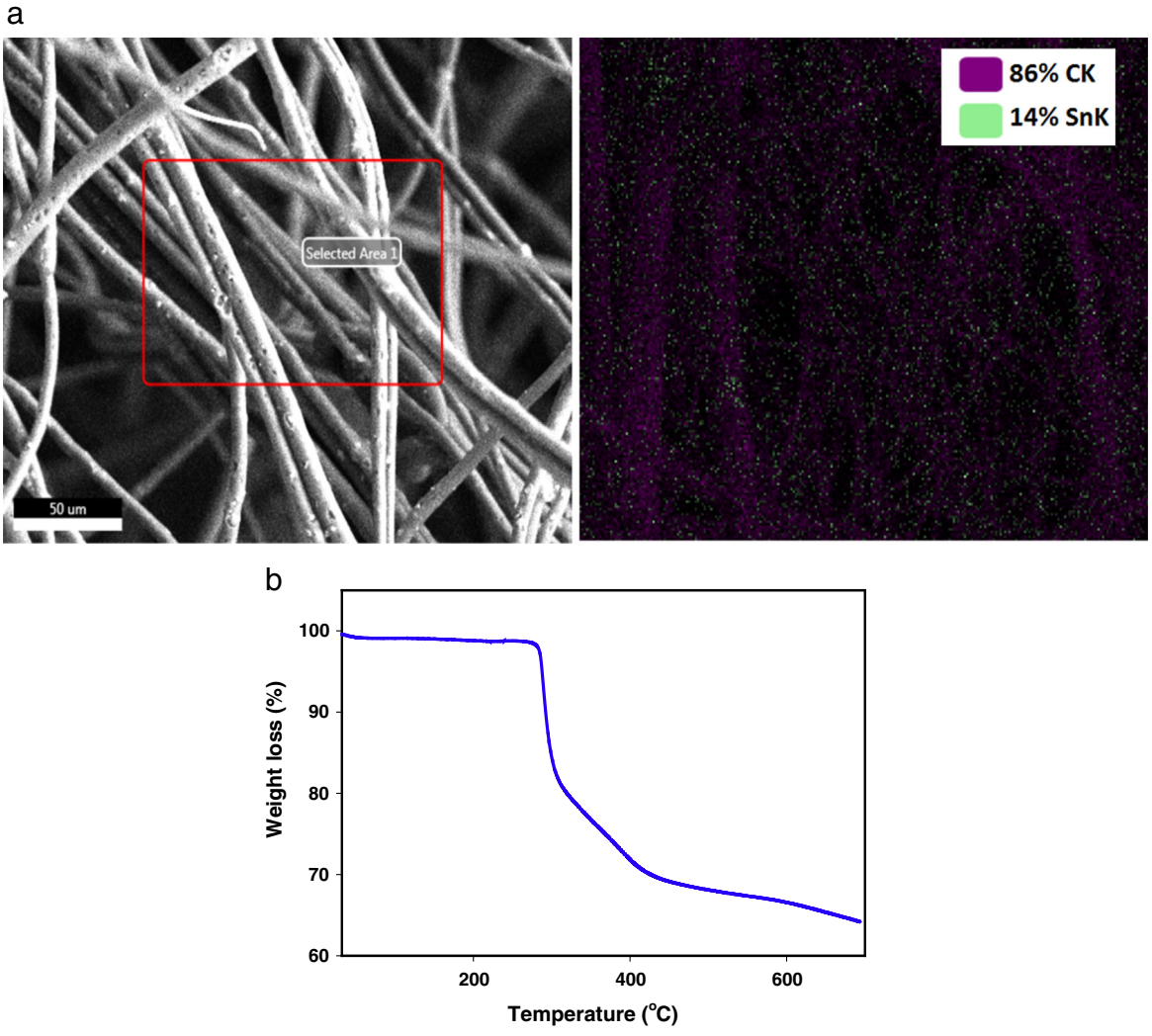

Fig. 4. a: SEM images and EDAX area mapping elemental analysis of the Sn/C composite nanofibers showing the nanofibers largely consisting of 86% atomic weight carbon and 14% atomic weight Sn particles in the carbon matrix. b: TGA thermogram of the Sn/PAN precursor nanofibers.

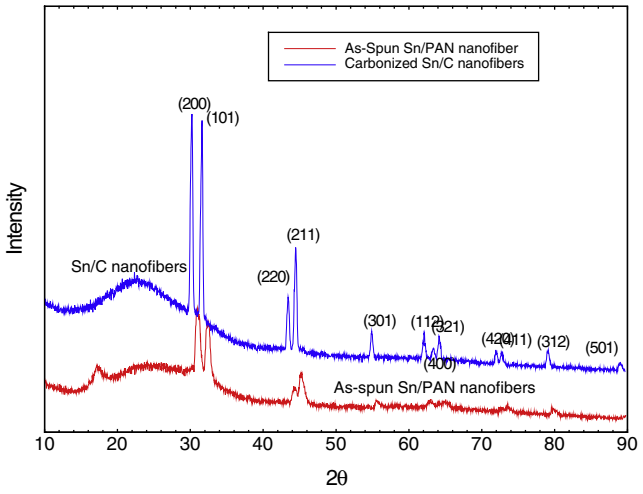

Fig. 5. XRD pattern of Sn/PAN precursor nanofibers and that of Sn/C composite nanofibers prepared from 15 wt.% Sn/PAN precursors at 800 °C. With indexed peak from JCPDS reference 00-004-0673.

indication of an increase in the interplanar layer spacing of the Sn/C crystal structure after the carbonization process. The narrowing of the FWHM values also pointed to disordering and increasing in the crystallite size of the Sn/C structure relative to the As-spun Sn/PAN nanofibers. The morphology, crystal growth and crystal structure of tin crystal present in the Sn/C composite nanofibers were shown to be independent of the Sn particle size (i.e. nano or micro) in the Sn/PAN solution precursor. Another difference, that was observed in the XRD patterns, was the variation of the relatively intensity ratio of peaks of the Sn/PAN precursor nanofibers and that of the Sn/C composite nanofibers which is an indication of enhanced crystallinity and large crystal size due largely to the carbonization process. Our XRD results are in agreement with those observed in the literature on Sn/C composite nanofiber anodes [65–68].

3.3. Surface analysis (XPS)

To evaluate the composition of the surface compounds on the Sn/PAN precursor nanofibers and that of the carbonized Sn/C nanofibers, a high resolution XPS analysis was carried out. To obtain enough information on the surface compounds, depth profiling instead of the regular point analysis was used. In Fig. 6a, the survey spectra of the Sn/PAN precursor nanofibers generally show peaks of Tin, carbon, and oxygen. The carbon peak is sharp, reflecting the predominate composition of the polymer (i.e. PAN) in the fibers. Those of Sn and oxygen are relatively small, especially the Sn peak. The relative weakness and sharpness of the Sn 3d peaks from the survey spectra reflected in the noisy spin orbital peaks of Sn 3d (i.e. $3d_{3/2}$ and $3d_{5/2}$) for the Sn/PAN precursor nanofibers. This could be attributed to the possibility of un-stabilized PAN polymer that crowded out the Sn nanoparticle peak that assigned to the spin–orbit components 3d5/2 at 495.3 eV. The oxygen (O 1s) peak had a little noisy signal compared to that observed in the carbonized Sn/C composite nanofibers. The carbon C 1s on the other hand shows one broad peak that was de-convoluted (Fig. 6b), into two peaks. Typically the binding energy of the C 1s with peak at 284.6 eV is often associated with the C-C bonds, which is attributed to the amorphous carbon phase or from the adventitious carbon. On the other hand, the peak at 285.6 eV was characteristic of the combination of C–O or the carboxyl (i.e. O–C═O) groups, that could have served as the nucleation points for the SnO_2 [69,70].

The XPS spectra for the Sn/C composite nanofiber prepared from Sn/PAN precursor nanofibers show distinct and sharp peaks of C 1s, Sn 3d and O 1s, with the Sn 3d showing two peaks associated with the spin–orbit components (3d3/2 and 3d5/2) of the Sn 3d peaks at binding energies ~495.3 and ~486.7 eV. (Fig. 6c). These results are consistent with those observed in the literature on Sn/C composite fiber anodes [67,71]. The splitting of the 3d doublet of Sn was 8.6 eV, indicating a probable valence state of Sn to be +4 [72]. This phenomenon is often attributed to the formation of SnO_2 compound in the Sn/C composite nanofiber structure [72]. The amount of SnO_2 in the carbonized Sn/C from the XRD results was small relative to the Sn metal content. The XPS spectra for the O1s scan show one peak at binding energy 530.6 eV which is assigned to the oxygen content in the fibers that could have been absorbed into the fibers from the atmosphere in form of moisture. This small moisture content in the fiber was observed as the fiber lost a small weight of ~3% at 96 °C according to the TGA results shown in Fig. 4b. The oxygen content could also be from the small content of SnO_2 in the fibers. These results thus point to a heterogeneous structure of the Sn/C composite nanofibers comprised of a small amount of SnO_2 particles and Sn metallic embedded in the carbon nanofiber matrix.

3.4. Electrochemical performance

3.4.1. Cyclic voltammogram for the Sn/C composite NF anode

Lithium storage properties of the Forcespun Sn/C composite nanofibers were evaluated in half-cell configuration between 0.0–3.0 V vs. Li/Li^+ at slow scan rate of 0.2 mV s^{-1}. Fig. 7 shows the cycle voltammetry (CV) curves of Sn (nanoparticles)/C composite nanofiber anode. During the first cathodic scan, the Sn/C composite NF anode exhibits a broad and sharp peak potential at ~0.38 V vs. Li/Li^+, which is attributed to the structural destruction of Sn/C and associated initial electrolyte decomposition [73]. Our CV results are in agreement with those reported on Sn/C nanocomposite anodes [74].

The decomposition reaction of the electrolyte solution with Li leads to the formation of the solid electrolyte interface (SEI) on the Sn/C anode at the interface between the Sn/C composite nanofiber anode and the electrolyte. In this case, the SEI layer will mainly consist of lithium carbonate and lithium alkyl species. The structural destruction of the small amount of SnO_2 species could lead to the formation of amorphous Li_2O according to the following partially reversible equilibrium equation;

$$SnO_2 + xLi^+ + xe^- \rightarrow Sn + 2Li_2O. \quad (1)$$

However, since the Li_2O typically occurs at higher potentials >0.75 V vs. Li/Li^+ during the cathodic sweep, which was not observed in Fig. 7, reaction (1) could not have occurred. Therefore the amount of SnO_2 in the electrode was considered insignificant. The presence of a peak potential at ~0.23 V vs. Li/Li^+ is associated with the reversible alloying formation process between the Sn and lithium according to reaction (2):

$$Sn + xLi^+ + xe^- \leftrightarrow Li_xSn, 0 \le x \le 4.4. \quad (2)$$

The peak potential of ~0.82 V vs. Li/Li^+ corresponds to the de-alloying reaction according to the reduction reaction above. During this de-alloying process, it is possible that electrochemically formed Sn nanoparticles could aggregate to form large clusters in order to reduce surface free energy. It is the formation of such large clusters that normally leads to the cracking of the electrode and the eventual increase in the cell internal resistance.

The storage/cycling performance of the Sn/C composite anode was investigated at room temperature. The cycle performance (i.e. charge/discharge cycling) was carried out at a voltage between 0.05 V and 3.0 V and at a current density of 100 mA/g for CNFs (i.e. prepared from PAN precursor) and Sn/C composite nanofiber anodes with different particle size of Sn (nano and submicron) were obtained for the first 50 cycles. The CNF anode shows an initial specific capacity of about 421 mA h g^{-1} (Fig. 8a), which is greater than the theoretical capacity

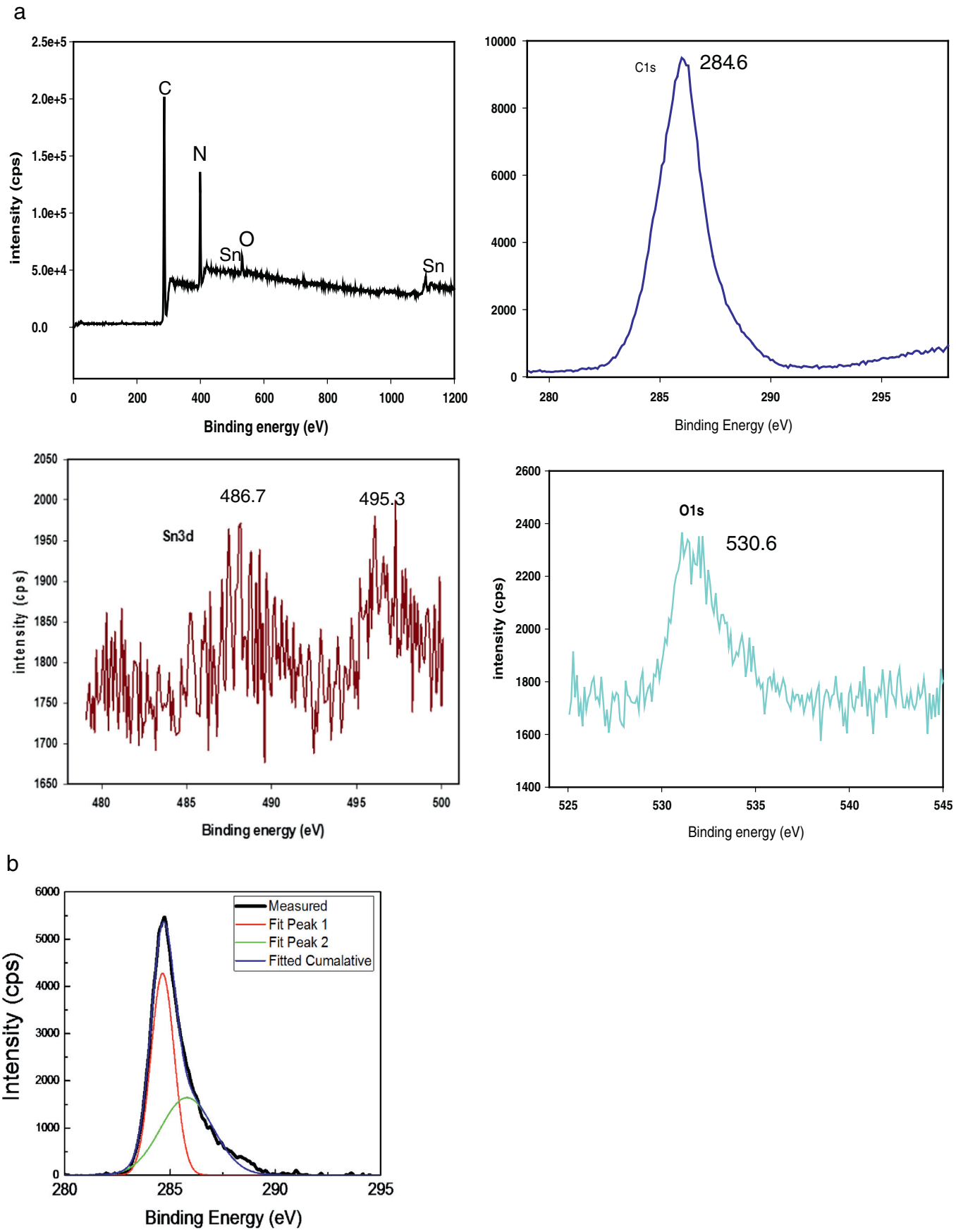

Fig. 6. a: XPS spectra of C 1s, O1s, and Sn3d and survey spectra for the Sn/PAN precursor nanofibers. b: De-convoluted peaks of the C1s, showing two peaks at 284.6 eV and 285.6 eV belonging to the adventitious carbon and the carboxyl group. c: XPS spectra of C 1s, O 1s, and Sn 3d for Sn/C composite nanofibers.

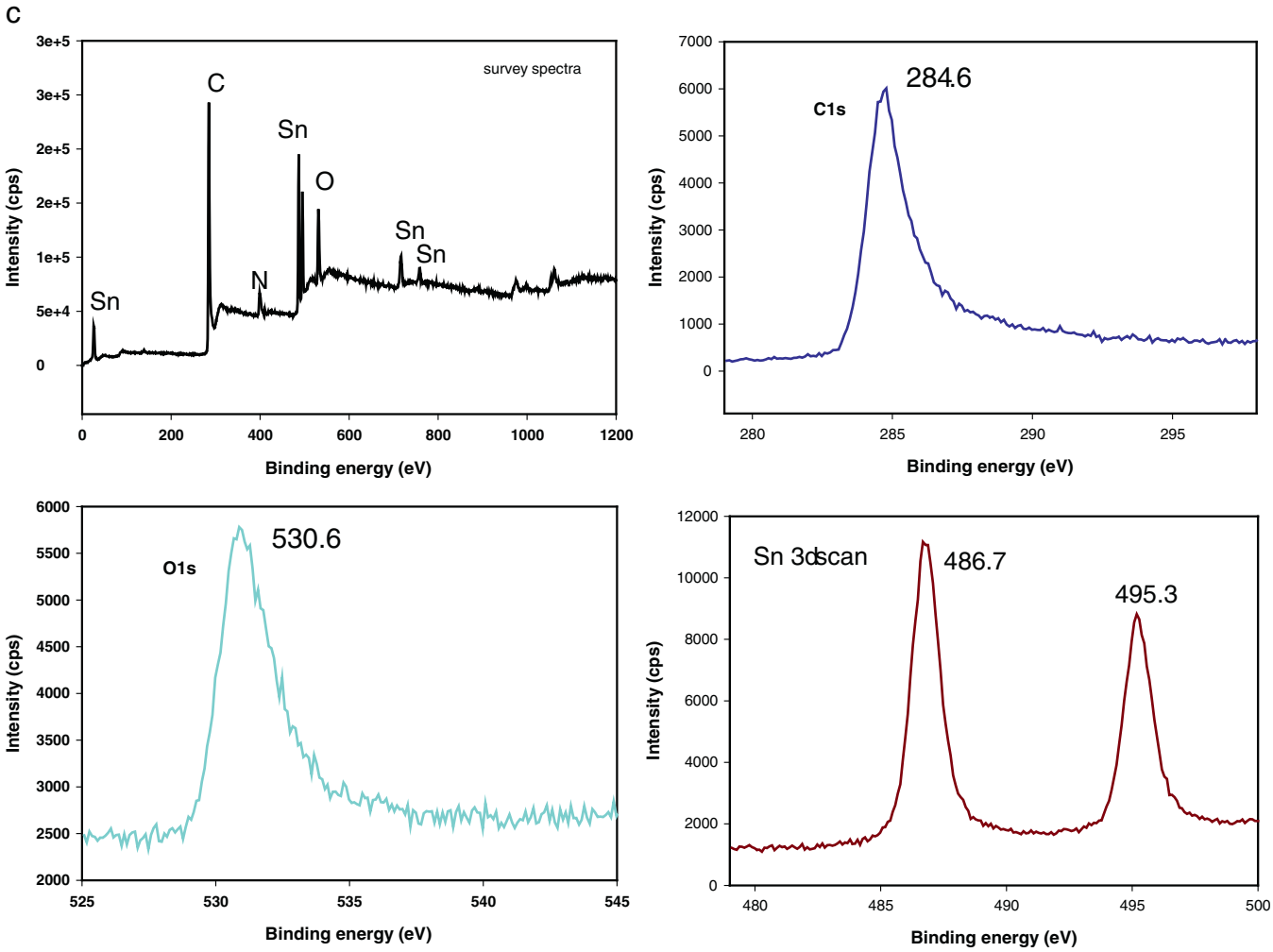

Fig. 6 (*continued*).

of graphite (372 mA h g^{-1}). This high capacity faded rapidly after the 1st cycle, which was attributed to the formation of the SEI layer. The rate of degradation of the specific capacity reduced significantly from the 5th to the 50th cycle and maintained a very flat capacity of about 297 mA h g^{-1} over 50 cycles (Fig. 9). For the Sn/C composite nanofiber anodes (nano and micro), the Sn in the carbon matrix initiated the general electrochemical reactions with lithium during the alloying process:

$$\begin{aligned} &Sn + xLi + xe^- \leftrightarrow Li_xSn (0 \le x \le 4.4) \\ &C + xLi^+ + xe^- \rightarrow Li_xC \end{aligned} \quad (3)$$

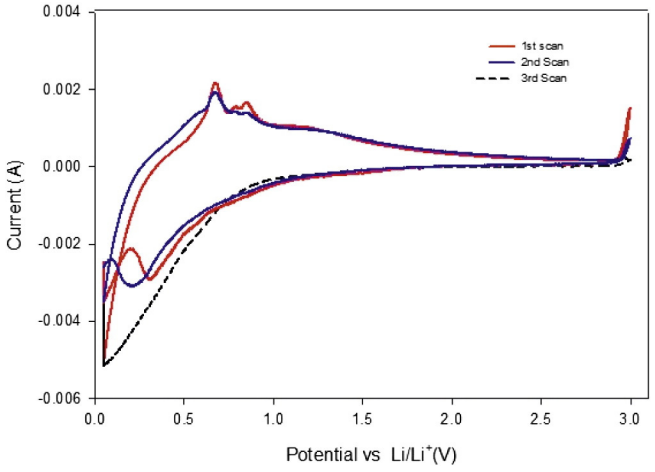

Fig. 7. Cyclic voltammogram (CV) curves of Sn (nanoparticles)/C composite nanofibers prepared from Sn/PAN precursor. Scan rate:0.2 mV s^{-1}.

This reaction produced initial specific charge capacities (lithium insertion) of 2586 mA h g^{-1} and 1578 mA h g^{-1}, at a current density of 50 mAg^{-1}, for the nano particle and micro particle Sn/C composite electrode, corresponding to Coulombic efficiencies of 41, and 75%, respectively (Fig. 8 b and c). These first charge capacities are remarkably higher than that reported in the literature [34,72,75] on Sn/C or SnO_2/C composite nanofiber anodes. There is a steady drop in the charge capacity (Lithium insertion) for both nano and submicron Sn/C composite nanofibers, which are consistent with results reported in literature [24,27,31,72]. The drastic drop in capacity for the Sn/C composite anode is usually associated with the inevitable irreversible loss of L^+ for the formation of the SEI layer. Unlike in many other battery chemistries such as the $Li_{x+1}FePO_4$ and $Li_xMn_{1-x}NiCoO_4$ cathodes where extra lithium is provided for the cathode to compensate for the SEI layer formation. Thereafter the charge capacity of Sn/C composite nanofiber anodes at 100 mA g^{-1} (nano and submicron) remains relatively steady over the 50 cycles (Fig. 8 b and c).

Fig. 9 shows the cycling performance of CNF and Sn/C (nano and submicron) composite anodes. These results indicate that the charge capacity (Li-insertion) of Sn (nanoparticle)/C composite anode rapidly

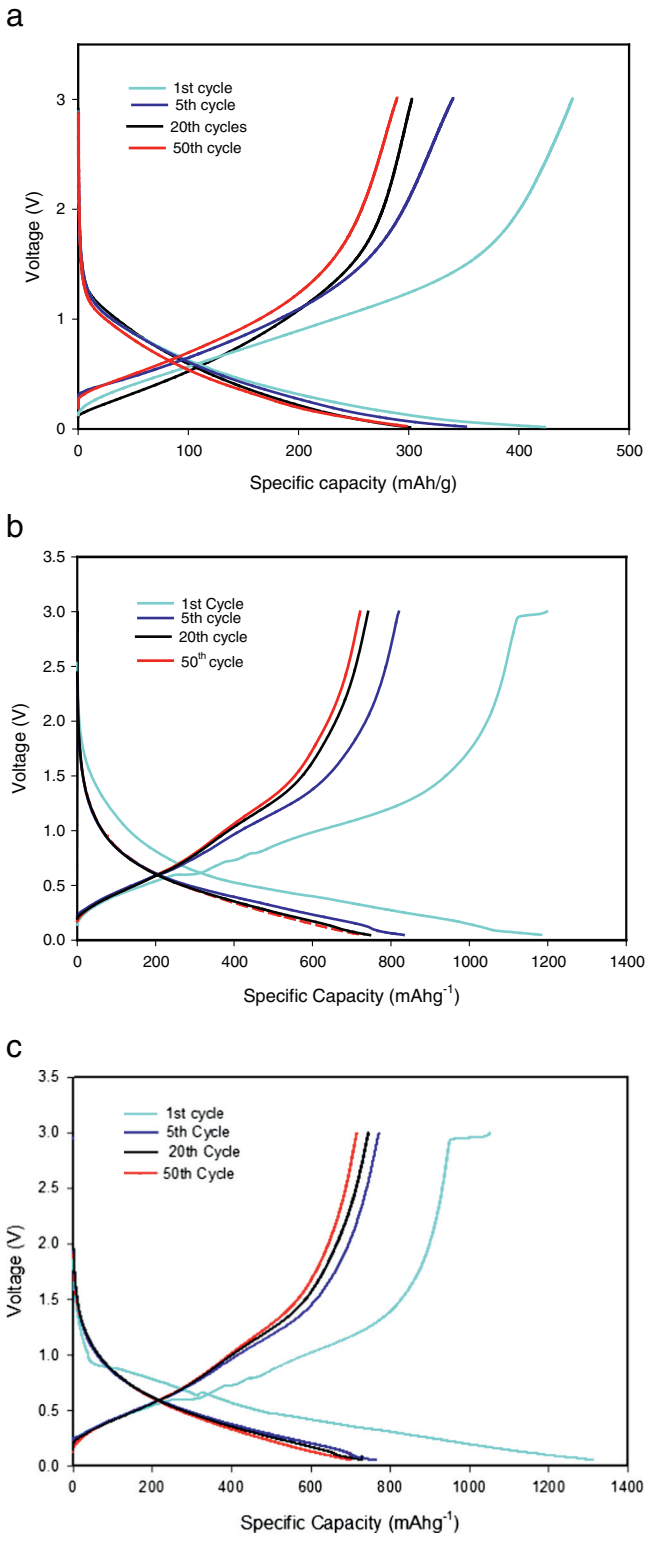

Fig. 8. a: Galvanostatic charge/discharge curves for CNFs made from PAN precursor nanofibers in the voltage range of 0.05–3.0 V (versus Li+/Li) at a current density of 100 mA g^{-1}. b: Charge/discharge curves for the Sn (nanoparticles)/C composite nanofiber anode in the voltage range of 0.05–3.0 V (versus Li+/Li) at a current density of 100 mA g^{-1}. c: Charge/discharge curves for the Sn (microparticles)/C composite nanofiber anode in the voltage range of 0.05–3.0 V (versus Li^+/Li) at current density of 100 mA g^{-1}.

decreases to about 921 mA h g^{-1} after the 2nd cycle. The drop in charge capacity continues up to the 10th cycle. After 50 cycles, this Sn/C composite anode still retains a charge capacity of 715 mA h g^{-1}. The cycle

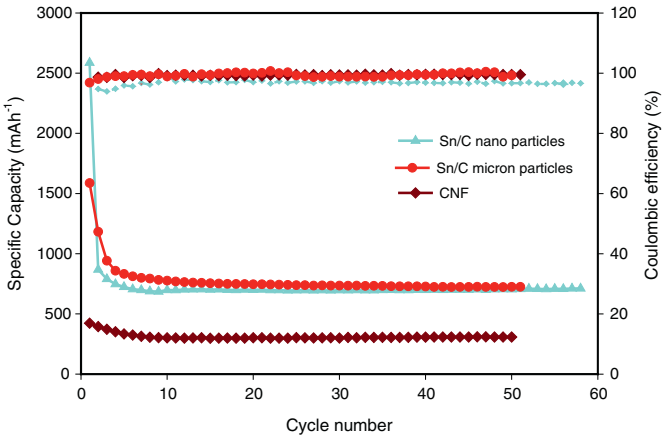

Fig. 9. Cycling performance of Sn (nanoparticle)/C and Sn (micro-particle)/C composite anodes prepared from Sn/PAN precursor nanofibers. For comparison, the results for CNFs made from PAN precursor nanofibers are also shown.

performance of the submicron Sn/C composite anode follows a similar trend as in the nanoparticle Sn/C composite anode. However, unlike the nano particle Sn/C composite electrode, the micro particle Sn/C composite anode delivers a specific charge capacity (lithium insertion) of 1152 mA h g^{-1} after the 2nd cycle. This Sn/C composite anode still retains a specific charge capacity of 724 mA h g^{-1} after 50 cycles with capacity retention of 82%. The Sn/C composite anodes display a Coulombic efficiency >95% after the second cycle (Fig. 9). Statistically, the subtle difference between the specific capacities of the two Sn/C composite nanofiber anodes is the same. The Sn nanoparticles with large surface area and high aspect ratio offer the Sn/C electrode more reactive sites for electrochemical reaction compared to the submicron particles, therefore, it is expected that the Sn (nanoparticles)/C composite anode should exhibit a better electrochemical performance than the Sn (micro-particles)/C composite anode. The subtle difference in the charge/discharge capacities for the submicron Sn/C composite anode is attributed to the large and evenly distributed pores on the fibers (Fig. 3f), which offers a much more buffering effect to accommodate the volume change during the alloying/de-alloying process. The stability of the Sn (nanoparticles)/C composite electrode was evaluated using different current densities, as shown in Fig. 10. The Sn (nano-particle)/C composite anode recorded a capacity of 716 mA h g^{-1} after the first cycle that faded a little up to the 3rd cycle and maintained a steadily capacity thereafter. For a higher current density of 500 mA/g, a much low capacity of about 427 mA h g^{-1} was observed, which stabilized after the

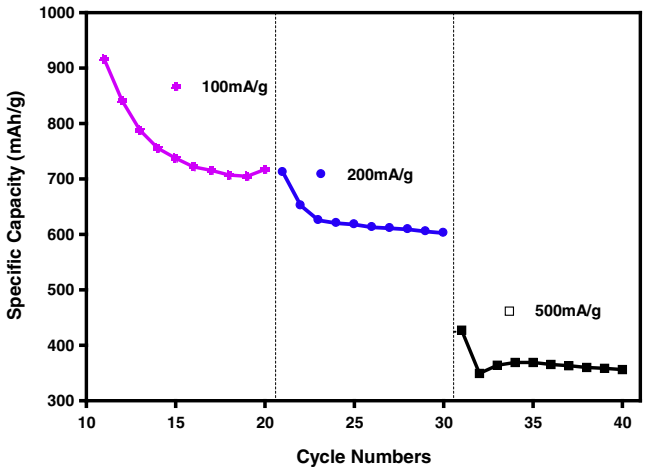

Fig. 10. Rate performance of the Sn (nano-particles)/C composite nanofiber anode at a current density of; 100 mA/g, 200 mA/g, and 500 mA/g over 10 cycles between 0.05–3.0 V.

Table 1
A comparison of the cycle performance of Sn/C composite nanofiber anodes reported in the literature (NFs were prepared by electrospinning).

Electrode chemistry	Flexible fibers?	Additive added	Charge capacity (mA h g^{-1})	Cycle number	Reference
Sn–Porous C	Yes	Mineral oil (Acros)	774	200	[75]
Sn/C	Yes	None	300	200	[75]
Sn/C	No	Acetylene black	626	50	[68]
SnO_2–NiO–C	No	None	620	80	[71]
Sn/C	Yes	None	450	25	[66]
SnO_2/C (carbon nanotubes)	No	Acetylene black	725	50	[55]
SnO_2/C	No	Super P Li (Timcal)	82	75	[36]
SnO_2/C	Yes	None	602	100	[27]
Sn/C	No	Super-P (MMM Carbon)	465	100	[21]

3rd cycle at a modest capacity of 342 mA h g^{-1}. The relatively higher capacity regardless of the particle size is most importantly due to the quality of the nanofiber produced using the Forcespinning method, which produced fibers that are uniform and capable of buffering the volume change associated with Sn/C composite anode during the charge/discharge process. Most results reported in literature on binder-free electrodes prepared by electrospinning and centrifugal spinning show [66,68,76] lower charge capacities that range from 400 to 650 mA h g^{-1} after 50 cycles. Table 1 shows some compilation/comparison of the cycle performance of Sn/C and SnO_2/C composite nanofiber anodes produced using the Electrospining process. Most of the results illustrated in Table 1 show a higher specific capacity than our results due to the fact that additives such as acetylene black were used to prepare the composite nanofiber anode which led to improve the electronic conductivity of electrode. The results from ground nanofibers (i.e. current collector based electrode) is even much lower except that from Shen et al. [75] who studied Sn (nanoparticle)/C porous nanofibers containing conductive carbon black as additive. In that work, a charge capacity (Li insertion) of 774 mA h g^{-1} at a current density of 0.8 $Ag^{-1}$was reported for the highly porous Sn/C composite nanofibers after 200 cycles. Shen et al. also reported results on the electrochemical performance of electrospun Sn/C composite nanofibers prepared from Sn/PAN precursor nanofibers (without additives) [75]. This Sn/C composite anode delivered charge capacities of 500 and 300 mA h g^{-1} (at 0.8 Ag^{-1}) after 50 and 200 cycles, respectively.(Table 1). Our results discussed in this work show that the Forcespun Sn/C composite anodes exhibit a better electrochemical performance than that reported on electrospun Sn/C composite anode (without additives) [75].

The Nyquist plots for the electrochemical impedance before and after cycling for both the submicron and the nanoparticle based Sn/C composite electrodes as shown in Fig. 11 was carried out to elucidate the associated electrochemical performance. The depressed semicircles in the region of high to middle frequency range, which represent the initial interfacial resistance and charge-transfer resistance, clearly show a slight variation in the impedance between the two electrodes. The submicron particle Sn/C composite anode shows a lower initial impedance compared to the nanoparticle Sn/C composite anode and a relatively small increase in the charge transfer resistance (i.e. from the shift to the right on the Z-real axis) was observed. After 50 cycles, there is an increase in the diameter of the semi-circle for both electrodes, with the nanoparticle Sn/C composite electrode having a slightly higher semicircle diameter. The increase in resistance at the electrode/electrolyte interface for the nanoparticle Sn/C composite cells affected the lithium ion kinetics at the interface which is correlated with the steady loss in cell capacity during the initial cycles. The improvement in electrochemical performances of the Sn/C composite nanofiber anode is attributed to the uniform dispersion of Sn particles in the carbon nanofiber that provided a large number of active sites for Li ion storage and shorter lithium ion transfer distance. Additionally, the uniform and porous fiber mat also provides a large surface area not only for reactive sites but also allows for ion and electron transport without the need for a current collector. All these attributes contribute immensely to the improved cycling performance of the Sn/C composite nanofiber anodes prepared from forceospun Sn/PAN precursor nanofibers.

4. Conclusions

Sn/C nanofiber composite anodes were produced by the Forcespinning of Sn nano and micro particles in PAN/DMF solutions followed by heat treatment (stabilization and carbonization steps).

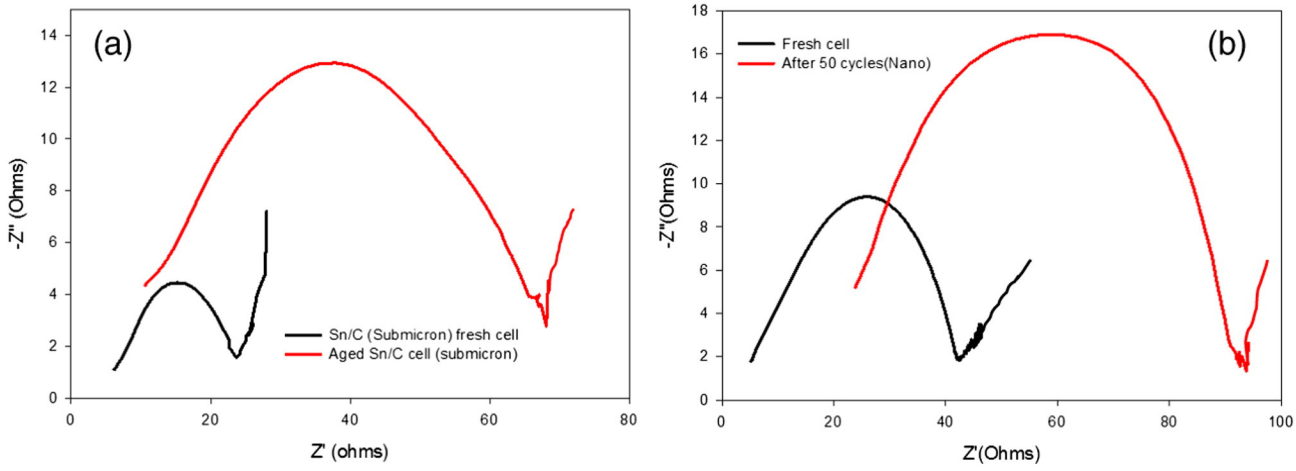

Fig. 11. Electrochemical impedance spectra obtained before and after cycling for both the submicron and the nanoparticle based Sn/C composite nanofiber anodes (a) Sn (microparticles)/C composite NFs and (b) Sn (nanoparticles)/C composite NFs.

Forcespinning is a new cost effective technique for the mass production of high quality of fibrous mats and it has proven to be a more efficient method to produce high quality PAN and Sn/PAN precursor nanofibers. Sn/C composite nanofibers that are porous with a large surface area for easy ion transport while acting as a buffer to reduce the volume expansion and extraction associated with alloying/se-alloying of the Sn particles with lithium. These properties of the Forcespun Sn/C composite anode translated into a better electrochemical performance including better cycling and rate performance as well as capacity retention compared to those prepared by electrospinning and centrifugal spinning. To the best of our knowledge, this is the first time to report results on the use of Forcespinning technology to produce composite nanofiber electrodes for lithium-ion batteries. The results from this work are thus the first step towards the use of this technology for the mass production of high quality nanofibers as binder-free electrodes for lithium ion batteries. The versatility of the Forcespinning process makes it suitable to extend its application to the production of nanofibrous mats for electrode material, separators as well as high quality nanofibers for electronics and biomedical applications.

Acknowledgments

This work was supported by the University of Texas System (STARS program) through the startup funding to M. Alcoutlabi. This research was also supported by NSF PREM award DMR-1523577: UTRGV-UMN Partnership for Fostering Innovation by Bridging Excellence in Research and Student Success.

References

[1] M. Alcoutlabi, G.B. McKenna, J. Phys. Condens. Matter 17 (15) (2005) R461–R524.
[2] V. Aravindan, et al., Electrochim. Acta 121 (0) (2014) 109–115.
[3] X. Liu, et al., J. Power Sources 272 (2014) 614–621.
[4] G.K. Simon, et al., J. Power Sources 196 (23) (2011) 10254–10257.
[5] Y. Zhao, et al., J. Power Sources 274 (0) (2015) 869–884.
[6] L.W. Ji, et al., Energy Environ. Sci. 4 (8) (2011) 2682–2699.
[7] M. Alcoutlabi, et al., AATCC Rev. 11 (6) (2011) 45–51.
[8] H. Honbo, et al., J. Power Sources 189 (1) (2009) 337–343.
[9] M. Rosso, et al., J. Power Sources 97-8 (2001) 804–806.
[10] J. Chen, et al., Electrochim. Acta 127 (0) (2014) 390–396.
[11] H. Park, et al., J. Power Sources 244 (0) (2013) 726–730.
[12] Q. Tian, et al., J. Power Sources 269 (0) (2014) 479–485.
[13] W. Ma, et al., J. Mater. Chem. A 3 (10) (2015) 5442–5448.
[14] C.T. Fleaca, F. Le Normand, Phys. E 56 (2014) 435–440.
[15] M.A. Hoque, et al., Electrochim. Acta 121 (0) (2014) 421–427.
[16] J.W. Wang, et al., Nano Lett. 13 (2) (2013) 709–715.
[17] B.-S. Lee, et al., J. Power Sources 199 (0) (2012) 53–60.
[18] J.-S. Bridel, et al., J. Power Sources 195 (7) (2010) 2036–2043.
[19] T. Inose, et al., J. Power Sources 162 (2) (2006) 1297–1303.
[20] A. Mukhopadhyay, B.W. Sheldon, Prog. Mater. Sci. 63 (2014) 58–116.
[21] I. Meschini, et al., J. Power Sources 226 (0) (2013) 241–248.
[22] C.-M. Chen, P.-Y. Shih, J. Mater. Res. 23 (10) (2008) 2668–2673.
[23] W.S. Kim, et al., J. Power Sources 225 (2013) 108–112.
[24] H. Jiang, et al., J. Mater. Sci. 50 (3) (2015) 1094–1102.
[25] X. Li, et al., Electrochim. Acta 147 (0) (2014) 40–46.
[26] D. Bresser, et al., Electrochim. Acta 128 (0) (2014) 163–171.
[27] M. Dirican, et al., J. Power Sources 264 (0) (2014) 240–247.
[28] J. Jia, et al., Electrochim. Acta 141 (0) (2014) 13–19.
[29] Z. Wang, G. Chen, D. Xia, J. Power Sources 184 (2) (2008) 432–436.
[30] C. Cui, et al., Mater. Lett. 143 (2015) 35–37.
[31] L. Lang, et al., ACS Appl. Mater. Interfaces 7 (17) (2015) 9098–9102.
[32] L. Wei, et al., J. Alloys Compd. 644 (2015) 742–749.
[33] Y. Zhong, et al., Appl. Surf. Sci. 332 (2015) 192–197.
[34] C.A. Bonino, et al., ACS Appl. Mater. Interfaces 3 (7) (2011) 2534–2542.
[35] B.-O. Jang, S.-H. Park, W.-J. Lee, J. Alloys Compd. 574 (2013) 325–330.
[36] T. Tran, et al., Electrochim. Acta 117 (0) (2014) 68–75.
[37] M. Alcoutlabi, et al., Macromolecules 44 (10) (2011) 3828–3839.
[38] M. Alcoutlabi, L. Banda, G.B. McKenna, Polymer 45 (16) (2004) 5629–5634.
[39] X. Zhang, et al., Polym. Rev. 51 (3) (2011) 239–264.
[40] D. Nan, et al., Electrochem. Commun. 34 (2013) 52–55.
[41] L.W. Ji, et al., Carbon 47 (14) (2009) 3346–3354.
[42] H. Chen, et al., Micro Nano Lett. 10 (2) (2015) 81–84.
[43] Y. Lu, et al., J. Power Sources 273 (2015) 502–510.
[44] M. Khamforoush, T. Asgari, Nano (2015) 10(2).
[45] F. Dabirian, S.A.H. Ravandi, A.R. Pishevar, Curr. Nanosci. 6 (5) (2010) 545–552.
[46] F. Dabirian, et al., J. Electrost. 69 (6) (2011) 540–546.
[47] F. Dabirian, S.A.H. Ravandi, A.R. Pishevar, Fibers Polym. 14 (9) (2013) 1497–1504.
[48] M. Yanilmaz, et al., J. Power Sources 273 (2015) 1114–1119.
[49] M. Yanilmaz, X.W. Zhang, Polymers 7 (4) (2015) 629–643.
[50] N.E. Zander, J. Appl. Polym. Sci. (2015) 132(2).
[51] K. Sarkar, et al., Mater. Today 13 (11) (2010) 12–14.
[52] Sarkar, K.L.a.K., inventors Super fine Fiber Creating Spinneret and Uses Thereof, in US Patent, U.p. Office, Editor 2009: USA.
[53] B.C. Weng, et al., Cellulose 22 (2) (2015) 1311–1320.
[54] B.C. Weng, et al., Polym. Eng. Sci. 55 (1) (2015) 81–87.
[55] D. Li, Y. Xia, Adv. Mater. 16 (14) (July 2004) 1151–1170, http://dx.doi.org/10.1002/adma.200400719.
[56] H. Lee, et al., J. Solid State Electrochem. 18 (9) (2014) 2451–2458.
[57] H. Lee, et al., J. Polym. Sci. B Polym. Phys. 51 (5) (2013) 349–357.
[58] H. Lee, et al., J. Appl. Polym. Sci. 129 (4) (2013) 1939–1951.
[59] L.W. Ji, et al., RSC Adv. 2 (1) (2012) 192–198.
[60] M. Alcoutlabi, et al., J. Mater. Sci. 48 (6) (2013) 2690–2700.
[61] Y. Li, et al., ECS Electrochem. Lett. 1 (2) (2012) A31–A33.
[62] A.M. Loordhuswamy, et al., Mater. Sci. Eng. C Mater. Biol. Appl. 42 (2014) 799–807.
[63] M.R. Badrossamay, et al., Biomaterials 35 (10) (2014) 3188–3197.
[64] V.A. Agubra, et al., J. Appl. Polym. Sci. (2016) 133(1).
[65] S. Kim, et al., J. Electroceram. 32 (4) (2014) 261–268.
[66] H.Y. Wang, et al., Electrochim. Acta 58 (2011) 44–51.
[67] X.J. Bai, et al., J. Alloys Compd. 628 (2015) 407–412.
[68] X. Xia, et al., Electrochim. Acta 121 (2014) 345–351.
[69] F. Ahimou, et al., J. Colloid Interface Sci. 309 (1) (2007) 49–55.
[70] Y. Zhang, L. Jiang, C. Wang, Nanoscale 7 (28) (2015) 11940–11944.
[71] Q. Yang, et al., Ceram. Int. 41 (9) (2015) 11213–11220.
[72] J. Mu, et al., J. Colloid Interface Sci. 356 (2) (2011) 706–712.
[73] Y.B. Cai, et al., Int. J. Green Energy 11 (8) (2014) 861–875.
[74] N. Zhang, et al., Nanoscale 6 (5) (2014) 2827–2832.
[75] Z. Shen, et al., J. Power Sources 278 (0) (2015) 660–667.
[76] H.K. Zhang, et al., Electrochim. Acta 59 (2012) 160–167.